

# Solving Large-scale Systems of Random Quadratic Equations via Stochastic Truncated Amplitude Flow

Gang Wang, *Student Member, IEEE*, Georgios B. Giannakis, *Fellow, IEEE*,  
and Jie Chen, *Senior Member, IEEE* \*

August 27, 2016

## Abstract

This paper develops a new algorithm, which we call *stochastic truncated amplitude flow* (STAF), to reconstruct an unknown  $n$ -dimensional (typically  $n$  very large) signal  $\mathbf{x}$  from  $m$  phaseless quadratic equations of the form  $\psi_i = |\langle \mathbf{a}_i, \mathbf{x} \rangle|$ . This problem, also known as phase retrieval, is *NP-hard* in general. Adopting an amplitude-based nonconvex formulation, STAF is an iterative solution algorithm comprising two stages: s1) The first stage employs a stochastic variance reduced gradient algorithm to solve for an orthogonality-promoting initialization; and, s2) the second stage iteratively refines the initialization using stochastic truncated amplitude-based gradient iterations. Both stages process a single equation per iteration, thus rendering STAF a simple, scalable, and fast algorithm amenable to large-scale implementations. Under the Gaussian random  $\mathbf{a}_i$  designs, we prove that STAF recovers exactly any signal  $\mathbf{x} \in \mathbb{R}^n$  exponentially fast from on the order of  $n$  quadratic equations. STAF is also robust vis-à-vis additive noise of bounded support. Simulated tests using the real Gaussian  $\mathbf{a}_i$  designs demonstrate that STAF empirically reconstructs any  $\mathbf{x} \in \mathbb{R}^n$  exactly from about  $2.3n$  magnitude-only measurements, outperforming the-state-of-arts and narrowing the gap from the information-theoretic number of quadratic equations  $m = 2n - 1$ . Extensive experiments using synthetic data and real images corroborate markedly improved performance of STAF over existing alternatives.

**Index terms**— Nonconvex optimization, phase retrieval, variance reduction, Kaczmarz algorithm.

## 1 Introduction

This paper considers the fundamental problem of reconstructing a general signal from the magnitude-only measurements, e.g., the magnitudes of the Fourier transform or any linear transform of the signal. This

---

\*Work in this paper was supported in part by NSF grants 1500713 and 1514056. G. Wang and G. B. Giannakis are with the Digital Technology Center and the ECE Dept., University of Minnesota, Minneapolis, MN 55455, USA. G. Wang is also with the School of Automation, Beijing Institute of Technology, Beijing 100081, P. R. China. J. Chen is with the School of Automation and State Key Laboratory of Intelligent Control and Decision of Complex Systems, Beijing Institute of Technology, Beijing 100081, P. R. China. E-mails: {gangwang,georgios}@umn.edu; chenjie@bit.edu.cn.

problem, also known as *phase retrieval* [1], arises in many fields of science and engineering ranging from X-ray crystallography [2], optics [3], as well as coherent diffraction imaging [4]. In such settings, due to physical limitations of optical detectors such as photosensitive films, charge-coupled device (CCD) cameras, and human eyes, one records only the intensity of the light (which describes the absolute counts of photons or electrons that strike the detectors) but loses the phase (where the wave peaks and troughs lie) [5]. It is known that when collecting the diffraction pattern at a large enough distance from the imaging plane, the field is given by the Fourier transform of the image (up to a known phase factor). Therefore, those optical devices in the far field essentially measure only the squared modulus of the Fourier transform of the object, whereas the phase of the incident light reaching the detector is missing. Nevertheless, very much information is contained in the Fourier phase. As is well known, the Fourier phase of an image encodes often more structural information than its Fourier magnitude. Recovering the phase from the magnitude-only measurements is thus of paramount practical relevance. Further details concerning recent advances in the theory and practice of phase retrieval can be found in the review [5].

Mathematically speaking, the generalized phase retrieval amounts to solving a system of phaseless quadratic equations taking the form

$$\psi_i = |\langle \mathbf{a}_i, \mathbf{x} \rangle|, \quad 1 \leq i \leq m \quad (1)$$

where  $\mathbf{x} \in \mathbb{R}^n$  or  $\mathbb{C}^n$  is the wanted unknown,  $\mathbf{a}_i \in \mathbb{R}^n$  or  $\mathbb{C}^n$  are known design/feature vectors, and  $\boldsymbol{\psi} := [\psi_1 \cdots \psi_m]^T$  is the observed data vector. Equivalently, (1) can also be given in its squared form as  $y_i = |\langle \mathbf{a}_i, \mathbf{x} \rangle|^2$ , where  $y_i := \psi_i^2$  are the intensity or the squared modulus.

In the classical discretized one-dimensional phase retrieval, the amplitude vector  $\boldsymbol{\psi}$  corresponds to the  $m$ -point (typically,  $m = 2n - 1$ ) Fourier transform of the length- $n$  signal  $\mathbf{x}$  [5]. It has been established using the fundamental theorem of algebra that there is no unique solution in the discretized 1D phase retrieval, even if one disregards trivial ambiguities resulting from operations that preserve Fourier magnitudes, including the global phase shift, conjugate inversion, and spatial shift [6]. In fact, there are up to  $2^{n-2}$  non-equivalent solutions beyond trivial ambiguities [6]. To overcome this ill-posedness of the 1D phase retrieval, different approaches have been suggested. Additional constraints on the unknown signal such as sparsity or non-negativity are enforced in [7, 8, 9, 10, 11]. Other viable options include introducing specific redundancy into measurements leveraging for example, the short-time Fourier transform [5], or masks [12], or simply assuming random measurements (e.g., Gaussian  $\mathbf{a}_i$  designs) [9, 1, 13, 14]. Hereafter, for concreteness of our theoretical results, this paper assumes random measurements  $\psi_i$  that are collected from the real-valued Gaussian model, which postulates independently and identically distributed (i.i.d.)  $\mathbf{a}_i \in \mathbb{R}^n \sim \mathcal{N}(\mathbf{0}, \mathbf{I}_n)$ . To demonstrate effectiveness of the proposed algorithm, experimental implementations for the complex-valued Gaussian model with i.i.d.  $\mathbf{a}_i \in \mathbb{C}^n \sim \mathcal{CN}(\mathbf{0}, \mathbf{I}_n) := \mathcal{N}(\mathbf{0}, \mathbf{I}_n/2) + j\mathcal{N}(\mathbf{0}, \mathbf{I}_n/2)$ , and using real images will be included as well.

It has been recently proved that when  $m \geq 2n - 1$  or  $m \geq 4n - 4$  generic measurements (e.g., from the Gaussian models) are acquired, the quadratic system in (1) determines uniquely an  $n$ -dimensional real- or complex-valued  $\mathbf{x}$  (up to a global sign or phase) [15, 16], respectively. In the real case,  $m = 2n - 1$  is also proved necessary for uniqueness [15]. Assuming the existence of a unique solution  $\mathbf{x}$ , our goal is to devise

efficient and scalable algorithms amenable to large-scale implementations: i) that provably reconstruct  $\mathbf{x}$  from a near-optimal number of phaseless quadratic equations as in (1); and ii), that feature in simultaneously low iteration and computational complexities as well as a linear convergence rate.

As a particular instance of nonconvex quadratic programming, the problem of solving phaseless quadratic equations subsumes as special cases various classical combinatorial optimization tasks involving Boolean variables (e.g., the *NP-Complete* stone problem [17, Section 3.4.1], [13]). Considering for instance the real-valued vectors  $\mathbf{a}_i$  and  $\mathbf{x}$ , this problem boils down to assigning signs  $s_i = \pm 1$ , such that the solution to the system of linear equations  $\langle \mathbf{a}_i, \mathbf{x} \rangle = s_i \sqrt{y_i}$ , denoted by  $\mathbf{z}$ , adheres to the given phaseless equations  $|\langle \mathbf{a}_i, \mathbf{z} \rangle| = \psi_i$ ,  $1 \leq i \leq m$ . It is clear that there are a total number  $2^m$  of different combinations of  $s_i$ 's, whereas only two combinations of these signs leads to  $\mathbf{x}$  up to a global sign. The complex scenario becomes even more complicated, in which instead of assigning a series of signs  $s_i$ 's, one looks for a collection of unimodular complex constants  $\sigma_i \in \mathbb{C}$  such that the resulting linear system and the original quadratic system are equivalent. Furthermore, solving phaseless quadratic equations has also found applications in estimating the mixture of linear regressions, in which the latent membership variables are viewed as the missing phases [18]. Indeed, it has been shown that reconstructing a discrete-time, finite-duration signal from its Fourier transform magnitudes is *NP-complete* [19]. Despite its practical relevance across various science and engineering fields, solving systems of phaseless quadratic equations is combinatorial in nature, and *NP-hard* in general.

*Notation.* Lower- (upper-) case boldface letters denote column vectors (matrices), and calligraphic symbols are reserved for sets. The symbol  $\mathcal{T}(\mathcal{H})$  stands for transposition (conjugate transposition), and  $\succeq$  for positive semidefinite matrices. For vectors,  $\|\cdot\|$  signifies the Euclidean norm; and  $\|\cdot\|_1$  or  $\|\cdot\|_\infty$  denotes the  $\ell_1$ - or  $\ell_\infty$ -norm, respectively. The symbol  $\lceil \cdot \rceil$  is the ceiling operation that returns the smallest integer greater than or equal to the given number. For a given function  $g(n)$  of integer  $n > 0$ ,  $\Theta(g(n))$  denotes the set of functions  $\Theta(g(n)) = \{f(n) : \text{there exist positive constants } C_1, C_2, \text{ and } n_0 \text{ such that } 0 \leq C_1 g(n) \leq f(n) \leq C_2 g(n) \text{ for all } n \geq n_0\}$ ; and likewise,  $\mathcal{O}(g(n)) = \{f(n) : \text{there exist positive constants } C \text{ and } n_0 \text{ such that } 0 \leq f(n) \leq C g(n) \text{ for all } n \geq n_0\}$ , and  $\Omega(g(n)) = \{f(n) : \text{there exist positive constants } C \text{ and } n_0 \text{ such that } 0 \leq C g(n) \leq f(n) \text{ for all } n \geq n_0\}$ .

## 1.1 Prior Art

Adopting the least-squares criterion (which would coincide with the maximum likelihood one when assuming an additive white Gaussian noise model), the task of tackling the quadratic system in (1) can be reformulated as that of minimizing the following *amplitude-based* empirical loss [8, 9, 14]

$$\underset{\mathbf{z} \in \mathbb{C}^n}{\text{minimize}} \quad \frac{1}{2m} \sum_{i=1}^m (\psi_i - |\mathbf{a}_i^H \mathbf{z}|)^2 \quad (2)$$

or, the *intensity-based* ones [20, 1, 13, 21, 22]

$$\underset{\mathbf{z} \in \mathbb{C}^n}{\text{minimize}} \quad \frac{1}{2m} \sum_{i=1}^m (y_i - |\mathbf{a}_i^H \mathbf{z}|^2)^2 \quad (3)$$

and

$$\underset{\mathbf{z} \in \mathbb{C}^n}{\text{minimize}} \quad \frac{1}{2m} \sum_{i=1}^m |\mathbf{a}_i^H \mathbf{z}|^2 - y_i \log(|\mathbf{a}_i^H \mathbf{z}|^2). \quad (4)$$

The latter would yield the maximum likelihood estimate when Poisson data are observed. Unfortunately, the three objective functions are nonconvex because of existence of the modulus in (2), or the quadratic terms in (3) and (4). It is well known that nonconvex functions may exhibit many stationary points, and minimizing nonconvex objectives is in general *NP-hard* and hence computationally intractable [23]. It is worth stressing that it is *NP-hard* to establish convergence to a local minimum due to the existence of complicated saddle point structures [23, 24].

Previous approaches for solving phaseless quadratic equations can be grouped into two categories: convex and nonconvex schemes. The nonconvex schemes consist of the ‘workhorse’ alternating projection algorithms commonly employed in practice such as Gerchberg-Saxton [25] and Fineup [8], AltMinPhase [9] and TAF [26, 14], trust-region and Gauss-Newton methods [21, 27], as well as the recently proposed Wirtinger-based variants including (truncated) Wirtinger flow (WF/TWF) [1], [13]. Stochastic or incremental counterparts including Kaczmarz and ITWF have been reported too [28], [22]. On the other hand, the convex alternatives typically rely upon the so-called *matrix-lifting* technique to derive semidefinite programming-based solvers such as PhaseLift [20], PhaseCut [29], and CoRK [30]. For the Gaussian model, comparisons between convex and nonconvex solvers in terms of their sample complexity and computational complexity to acquire an  $\epsilon$ -accurate solution are delineated in Table 1.

Table 1: Comparisons of Different Algorithms

Algorithm	Sample complexity $m$	Computational complexity
PhaseLift [20]	$\mathcal{O}(n)$	$\mathcal{O}(n^3/\epsilon^2)$
PhaseCut [29]	$\mathcal{O}(n)$	$\mathcal{O}(n^3/\sqrt{\epsilon})$
AltMinPhase [9]	$\mathcal{O}(n \log n (\log^2 n + \log(1/\epsilon)))$	$\mathcal{O}(n^2 \log n (\log^2 n + \log^2(1/\epsilon)))$
WF [1]	$\mathcal{O}(n \log n)$	$\mathcal{O}(n^3 \log n \log(1/\epsilon))$
TAF [14], TWF [13], ITWF [22]	$\mathcal{O}(n)$	$\mathcal{O}(n^2 \log(1/\epsilon))$
This paper	$\mathcal{O}(n)$	$\mathcal{O}(n^2 \log(1/\epsilon))$

## 1.2 This Paper

Considering an amplitude-based nonconvex formulation, this paper puts forth a new algorithm, referred to as *stochastic truncated amplitude flow* (STAF). STAF is an iterative solution algorithm that builds upon but considerably broadens the scope of the state-of-the-art TAF [14]. Specifically, STAF operates in two stages: Stage one employs a variance-reduced stochastic optimization algorithm to obtain an orthogonality-promoting initialization, whereas the second stage applies stochastic truncated amplitude-based iterations to refine the initial estimate. Our approach is shown to be able to reconstruct any  $n$ -dimensional real-/complex-valued signal  $\mathbf{x}$  from a nearly minimal number of magnitude-only measurements in linear time. Albeit achieving the

same order-optimal sample and computational complexities as TAF [14] and (I)TWF [13, 22], STAF has two advantages. Firstly, STAF enjoys  $\mathcal{O}(n)$  iteration complexity in both initialization and refinement stages, which is order-optimal and improves over  $\mathcal{O}(n^2)$  in the state-of-the-arts. Although ITWF adopted an incremental gradient method to achieve  $\mathcal{O}(n)$  iteration complexity at the second stage, its first stage relies on the gradient-type power method of iteration complexity  $\mathcal{O}(n^2)$  to obtain a truncated spectral initialization [22]. Moreover, as will be demonstrated by our simulated tests, STAF outperforms the state-of-the-art algorithms including TAF, ITWF, and (T)WF on both synthetic data and real images in terms of both exact recovery performance and convergence speed. Specifically for the real-valued Gaussian model, STAF empirically reconstructs any real-valued  $n$ -dimensional signal  $\mathbf{x} \in \mathbb{R}^n$  from a number  $m \approx 2.3n$  of magnitude measurements, which are close to the information-theoretic limit of  $m = 2n - 1$ . In sharp contrast, the existing alternatives such as TAF, ITWF, and (T)WF typically require a few times more measurements to achieve exact recovery. Markedly improved performance is also witnessed for STAF when the complex-valued Gaussian model and coded diffraction patterns of real images [12] are employed.

*Paper outline.* The rest of the paper is outlined as follows. Section 2 first reviews the truncated amplitude flow (TAF) algorithm, and subsequently motivates and derives the two stages of the proposed STAF algorithm. Section 3 summarizes STAF, and establishes its theoretical performance. Extensive tests comparing STAF with state-of-the-art approaches on both synthetic data and real images are presented in Section 4. Finally, main proofs are given in Section 5, and technical details can be found in Appendix.

## 2 Algorithm: Stochastic Truncated Amplitude Flow

In this section, TAF is first reviewed, and its limitations for large-scale applications are pointed out. To tackle those challenges faced by TAF, simple, scalable, and fast stochastic gradient descent (SGD)-type algorithms for both the initialization and gradient refinement stages are developed to yield our STAF.

To begin with, a number of basic concepts are introduced. Define the Euclidean distance of any estimate  $\mathbf{z}$  to the solution set as follows:  $\text{dist}(\mathbf{z}, \mathbf{x}) := \min \|\mathbf{z} \pm \mathbf{x}\|$  for real-valued signals, and  $\text{dist}(\mathbf{z}, \mathbf{x}) := \min_{\phi \in [0, 2\pi)} \|\mathbf{z} - \mathbf{x}e^{i\phi}\|$  for complex ones [1]. Define also the indistinguishable global phase constant in the real case as

$$\phi(\mathbf{z}) := \begin{cases} 0, & \|\mathbf{z} - \mathbf{x}\| \leq \|\mathbf{z} + \mathbf{x}\|, \\ \pi, & \text{otherwise.} \end{cases} \quad (5)$$

Henceforth, letting  $\mathbf{x}$  be any solution of the given system of quadratic equations in (1), we assume that  $\phi(\mathbf{z}) = 0$ ; otherwise,  $\mathbf{z}$  is replaced by  $e^{-j\phi(\mathbf{z})}\mathbf{z}$ , but for brevity of exposition, the phase adaptation term  $e^{-j\phi(\mathbf{z})}$  shall be dropped whenever it is clear from the context.

### 2.1 Truncated Amplitude Flow

In this section, the two stages of TAF are detailed [14]. In stage one, TAF employs power iterations to compute an orthogonality-promoting initialization, while the second stage refines the initialization via gradient-type

iterations. The orthogonality-promoting initialization builds upon a hidden fundamental characteristic in high-dimensional spaces, which asserts that high-dimensional random vectors are almost always nearly orthogonal to each other [31]. Its core idea relies on approximating the unknown  $\mathbf{x}$  by a vector  $\mathbf{z}_0 \in \mathbb{R}^n$  most orthogonal to a carefully selected subset of design vectors  $\{\mathbf{a}_i\}_{i \in \mathcal{I}_0}$ , with the index set  $\mathcal{I}_0 \subseteq [m] := \{1, 2, \dots, m\}$ . It is well known that the geometric relationship between any nonzero vectors  $\mathbf{p} \in \mathbb{R}^n$  and  $\mathbf{q} \in \mathbb{R}^n$  can be captured by their squared normalized inner-product defined as  $\cos^2 \theta := \frac{|\langle \mathbf{p}, \mathbf{q} \rangle|^2}{\|\mathbf{p}\|^2 \|\mathbf{q}\|^2}$ , where  $\theta \in [0, \pi]$  signifies the angle between  $\mathbf{p}$  and  $\mathbf{q}$ . Intuitively, the smaller  $\cos^2 \theta$  is, the more orthogonal the two vectors are. Assume with no loss of generality that  $\|\mathbf{x}\| = 1$ . Upon obtaining the squared normalized inner-products for all pairs  $\{(\mathbf{a}_i, \mathbf{x})\}_{i=1}^m$ , collectively denoted by  $\{\cos^2 \theta_i\}_{i=1}^m$  with  $\theta_i$  denoting the angle between  $\mathbf{a}_i$  and  $\mathbf{x}$ , the orthogonality-promoting initialization constructs  $\mathcal{I}_0$  by including the indices of  $\mathbf{a}_i$ 's that produce one of the smallest  $|\mathcal{I}_0|$  normalized inner-products. Precisely,  $\mathbf{z}_0$  can be found by solving

$$\underset{\|\mathbf{z}\|=1}{\text{minimize}} \quad \mathbf{z}^\top \left( \frac{1}{|\mathcal{I}_0|} \sum_{i \in \mathcal{I}_0} \frac{\mathbf{a}_i \mathbf{a}_i^\top}{\|\mathbf{a}_i\|^2} \right) \mathbf{z} \quad (6)$$

where  $|\mathcal{I}_0|$  is on the order of  $n$ . To be precise, as shown in [14, Theorem 1], one requires for exact recovery of TAF that  $m \geq c_1 |\mathcal{I}_0| \geq c_2 n$  holds for certain numerical constants  $c_1, c_2 > 0$ . Tackling problem (6) entails finding the smallest eigenvalue and the associated eigenvector of  $\mathbf{Y}_0 := \frac{1}{|\mathcal{I}_0|} \sum_{i \in \mathcal{I}_0} \frac{\mathbf{a}_i \mathbf{a}_i^\top}{\|\mathbf{a}_i\|^2} \succeq \mathbf{0}$ . Nevertheless, to avoid the  $\mathcal{O}(n^3)$  computational complexity of computing the eigenvector associated with the smallest eigenvalue as in (6), an application of the standard concentration result  $\sum_{i=1}^m \frac{\mathbf{a}_i \mathbf{a}_i^\top}{\|\mathbf{a}_i\|^2} \approx \frac{m}{n} \mathbf{I}_n$  simplifies that to computing the principal eigenvector of  $\bar{\mathbf{Y}}_0 := \frac{1}{|\bar{\mathcal{I}}_0|} \sum_{i \in \bar{\mathcal{I}}_0} \frac{\mathbf{a}_i \mathbf{a}_i^\top}{\|\mathbf{a}_i\|^2}$ , where  $\bar{\mathcal{I}}_0$  is the complement of  $\mathcal{I}_0$  in  $[m]$ . Upon collecting  $\{\mathbf{a}_i\}_{i \in \bar{\mathcal{I}}_0}$  into an  $n \times |\bar{\mathcal{I}}_0|$  data matrix  $\mathbf{D}$ , one can rewrite  $\bar{\mathbf{Y}}_0 = \mathbf{D} \mathbf{D}^\top$  to yield the following principal component analysis (PCA) problem

$$\tilde{\mathbf{z}}_0 := \arg \max_{\|\mathbf{z}\|=1} \frac{1}{|\bar{\mathcal{I}}_0|} \mathbf{z}^\top \mathbf{D} \mathbf{D}^\top \mathbf{z}. \quad (7)$$

On the other hand, if  $\|\mathbf{x}\| \neq 1$ , the estimate  $\tilde{\mathbf{z}}_0$  is scaled by  $\sqrt{\frac{1}{m} \sum_{i=1}^m y_i}$ , a norm estimate of  $\mathbf{x}$  to yield  $\mathbf{z}_0 := \sqrt{\frac{1}{m} \sum_{i=1}^m y_i} \tilde{\mathbf{z}}_0$ . Further details can be found in [14, Section II.B].

When the signal dimension  $n$  is modest, problem (7) can be solved exactly by a full singular value decomposition (SVD) of  $\mathbf{D}$  [32]. Yet it has a running time  $\mathcal{O}(\min\{n^2 |\bar{\mathcal{I}}_0|, n \bar{\mathcal{I}}_0^2\})$  (or simply  $\mathcal{O}(n^3)$  because  $|\bar{\mathcal{I}}_0|$  is required to be on the order of  $n$ ), which grows prohibitive in large-scale applications. A common alternative called power method tabulated in Algorithm 1 was employed in [14, 1, 13, 22] to compute an initial estimate [32]. Power method, on the other hand, involves a matrix-vector multiplication  $\bar{\mathbf{Y}}_0 \mathbf{u}_t$  per iteration, to yield iteration complexity of  $\mathcal{O}(n |\bar{\mathcal{I}}_0|)$  or  $\mathcal{O}(n^2)$  by passing through the selected data  $\{\mathbf{a}_i\}_{i \in \bar{\mathcal{I}}_0}$ . Furthermore, to produce an  $\epsilon$ -accurate solution, it entails a runtime of [32]

$$\mathcal{O} \left( \frac{1}{\delta} n |\bar{\mathcal{I}}_0| \log(1/\epsilon) \right) \quad (8)$$

depending on the eigengap  $\delta > 0$ , which is defined to be the gap between the largest and the second largest eigenvalues of  $\bar{\mathbf{Y}}_0$  normalized by the largest one [32]. It is clear that when the eigengap  $\delta$  is small, the required

runtime  $\mathcal{O}(n|\bar{\mathcal{I}}_0| \log(1/\epsilon)/\delta)$  of power method would be equivalent to many passes over the entire data, and this could be prohibitive for large datasets [33]. Hence, power method may not be appropriate for computing the initialization in large-scale applications, particularly those involving small eigengaps.

---

**Algorithm 1** Power method [32]

---

- 1: **Input:** Matrix  $\bar{\mathbf{Y}}_0 = \mathbf{D}\mathbf{D}^\mathcal{T}$ .
  - 2: **Initialize** a unit vector  $\mathbf{u}_0 \in \mathbb{R}^n$  randomly.
  - 3: **For**  $t = 0$  **to**  $T - 1$  **do**  
 $\mathbf{u}_{t+1} = \frac{\bar{\mathbf{Y}}_0 \mathbf{u}_t}{\|\bar{\mathbf{Y}}_0 \mathbf{u}_t\|}.$
  - 4: **End For**
  - 5: **Output:**  $\tilde{\mathbf{z}}_0 = \mathbf{u}_T$ .
- 

The second stage of TAF relies on truncated gradient iterations of the amplitude-based cost function (4). Precisely, with  $t \geq 0$  specifying the iteration number, the truncated gradient stage starts with the initial estimate  $\mathbf{z}_0$ , and operates in the following iterative fashion

$$\mathbf{z}_{t+1} = \mathbf{z}_t - \frac{\mu}{m} \sum_{i \in \mathcal{I}_{t+1}} \left( \mathbf{a}_i^\mathcal{T} \mathbf{z}_t - \psi_i \frac{\mathbf{a}_i^\mathcal{T} \mathbf{z}_t}{|\mathbf{a}_i^\mathcal{T} \mathbf{z}_t|} \right) \mathbf{a}_i, \quad t = 0, 1, \dots \quad (9)$$

where the index set responsible for the gradient regularization is given as [14]

$$\mathcal{I}_{t+1} := \left\{ 1 \leq i \leq m \mid \left| \frac{\mathbf{a}_i^\mathcal{T} \mathbf{z}_t}{|\mathbf{a}_i^\mathcal{T} \mathbf{x}|} \right| \geq \frac{1}{1 + \gamma} \right\}, \quad t = 0, 1, \dots \quad (10)$$

The truncation indeed amounts to including only those components having  $\mathbf{z}_t$  sufficiently away from the sign-change hyperplane  $\mathbf{a}_i^\mathcal{T} \mathbf{z}_t = 0$ , which provably eliminates the erroneously estimated signs ( $\frac{\mathbf{a}_i^\mathcal{T} \mathbf{z}_t}{|\mathbf{a}_i^\mathcal{T} \mathbf{z}_t|} \neq \frac{\mathbf{a}_i^\mathcal{T} \mathbf{x}}{|\mathbf{a}_i^\mathcal{T} \mathbf{x}|}$ ) with high probability. Its extreme power in the real-valued Gaussian model has been well-documented in [14].

## 2.2 Variance-reduced Orthogonality-promoting Initialization

This section first presents some empirical evidence showing that small eigengaps appear commonly in the orthogonality-promoting initialization approach. Figure 1 plots empirical eigengaps of  $\bar{\mathbf{Y}}_0 \in \mathbb{R}^{n \times n}$  under the real- and complex-valued Gaussian models from 100 Monte Carlo realizations under default parameters of TAF, where  $n = 10,000$  is fixed, and the ratio  $m/n$  the number of equations and unknowns increases by 0.2 from 1 to 6. As shown in Fig. 1, the eigengaps of  $\bar{\mathbf{Y}}_0$  of the orthogonality-promoting initialization in [14, Algorithm 1] are rather small particularly for small  $m/n$  close to the information limit 2. Using power iterations in Algorithm 1 of runtime  $\mathcal{O}(n|\bar{\mathcal{I}}_0| \log(1/\epsilon)/\delta)$  in (8) thus entails many passes over the entire data due to a small eigengap factor of  $1/\delta$ , which may not perform well in the presence of large dimensions common in imaging applications [33]. On the other hand, instead of using the deterministic power method, stochastic (incremental) algorithms have been developed in [34, 33]. These algorithms perform a much cheaper update per iteration by choosing some  $i_t \in \bar{\mathcal{I}}_0$  either uniformly at random or in a cyclic manner,

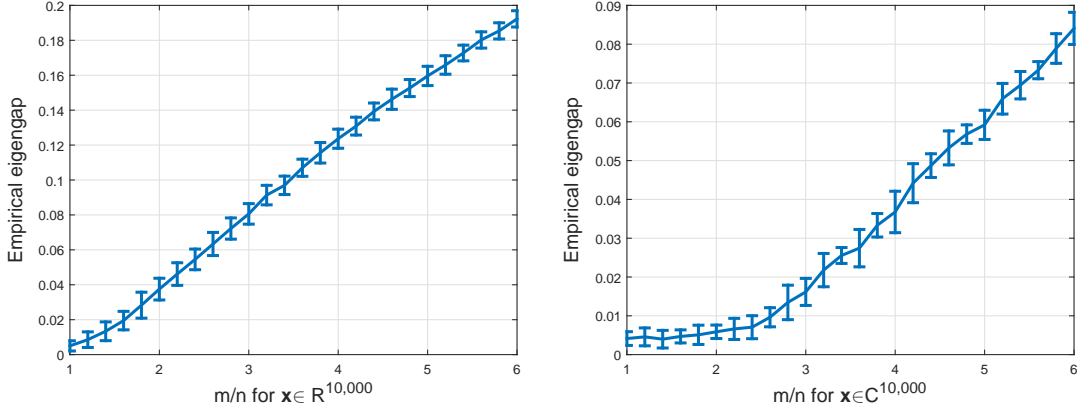


Figure 1: The eigengap  $\delta$  of  $\bar{\mathbf{Y}}_0 \in \mathbb{R}^{n \times n}$  averaging over 100 Monte Carlo realizations for  $n = 10,000$  fixed and  $m/n$  varying by 0.2 from 1 to 6. Left: The real-valued Gaussian model with  $\mathbf{x} \sim \mathcal{N}(\mathbf{0}, \mathbf{I}_n)$ ,  $\mathbf{a}_i \sim \mathcal{N}(\mathbf{0}, \mathbf{I}_n)$ , where  $n = 10^4$ . Right: The complex-valued Gaussian model with  $\mathbf{x} \sim \mathcal{CN}(\mathbf{0}, \mathbf{I}_n)$ ,  $\mathbf{a}_i \sim \mathcal{CN}(\mathbf{0}, \mathbf{I}_n)$ , where  $n = 10^4$ .

and updating the current iterate using only  $\mathbf{a}_{i_t}$ . They are shown to have iteration complexity of  $\mathcal{O}(n)$ , very appealing to large-scale applications. Building on recent advances in accelerating stochastic optimization schemes [35], a variance-reduced principal component analysis (VR-PCA) algorithm was proposed in [33]. VR-PCA performs cheap stochastic iterations, yet its total runtime is  $\mathcal{O}(n(\bar{\mathcal{L}}_0 + 1/\delta^2) \log(1/\epsilon))$  which depends also logarithmically on the solution accuracy  $\epsilon > 0$ . This is in sharp contrast to the standard SGD variant Oja’s algorithm, whose runtime, however, depends on  $1/\epsilon$  [34]. For the considered large-scale phase retrieval in most imaging applications, this paper advocates using the state-of-the-art algorithm VR-PCA to solve the orthogonality-promoting initialization problem in (7). In this direction, we refer to the resulting solution algorithm at the initialization stage as the *variance-reduced orthogonality-promoting initialization* (VR-OPI), which is summarized in Algorithm 2 next. Specifically, VR-OPI is a double-looped algorithm with a single execution of the inner loop referred to as an iteration and each execution of the outer loop as an epoch. In practice, the algorithm consists of a number  $S$  of epochs, while each epoch runs  $T$  (typically taken to be the data size  $|\bar{\mathcal{L}}_0|$ ) iterations.

Although effecting simple stochastic iterations, VR-OPI still enjoys a linear convergence rate under standard conditions. The following results adopted from [33, Theorem 1] establish linear convergence rate of VR-OPI.

**Proposition 1** ([33]). *Letting  $\mathbf{v}_1 \in \mathbb{R}^n$  be an eigenvector of  $\bar{\mathbf{Y}}_0$  associated with the largest eigenvalue  $\lambda_1$ . Assuming that  $\max_{i \in [m]} \|\mathbf{a}_i\|^2 \leq r := 2.3n$  (which holds with probability at least  $1 - me^{-n/2}$ ), the two largest eigenvalues of  $\bar{\mathbf{Y}}_0$  are  $\lambda_1 > \lambda_2 > 0$  with eigengap  $\delta = (\lambda_1 - \lambda_2)/\lambda_1$ , and  $\langle \tilde{\mathbf{u}}_0, \mathbf{v}_1 \rangle \geq 1/\sqrt{2}$ . Fix any*



---

**Algorithm 2** Variance-reduced orthogonality-promoting initialization (VR-OPI) [33]

---

- 1: **Input:** Data matrix  $D = \{\mathbf{a}_i\}_{i \in \bar{\mathcal{I}}_0}$ , step size  $\eta = 20/m$ , as well as the number of epochs  $S = 100$ , and the epoch length  $T = |\bar{\mathcal{I}}_0|$  (by default).
  - 2: **Initialize** a unit vector  $\tilde{\mathbf{u}}_0 \in \mathbb{R}^n$  randomly.
  - 3: **For**  $s = 0$  **to**  $S - 1$  **do**  
 $\mathbf{w} = \frac{1}{|\bar{\mathcal{I}}_0|} \sum_{i \in \bar{\mathcal{I}}_0} \mathbf{a}_i (\mathbf{a}_i^\top \tilde{\mathbf{u}}_s)$   
 $\mathbf{u}_1 = \tilde{\mathbf{u}}_s$ .
  - 4: **For**  $t = 0$  **to**  $T - 1$  **do**  
Pick  $i_t \in \bar{\mathcal{I}}_0$  uniformly at random  
 $\boldsymbol{\nu}_{t+1} = \mathbf{u}_t + \eta [\mathbf{a}_{i_t} (\mathbf{a}_{i_t}^\top \mathbf{u}_t - \mathbf{a}_{i_t}^\top \tilde{\mathbf{u}}_s) + \mathbf{w}]$   
 $\mathbf{u}_{t+1} = \frac{\boldsymbol{\nu}_{t+1}}{\|\boldsymbol{\nu}_{t+1}\|}$ .
  - 5: **End For**  
 $\tilde{\mathbf{u}}_{s+1} = \mathbf{u}_T$ .
  - 6: **End For**
  - 7: **Output:**  $\tilde{\mathbf{z}}_0 = \mathbf{u}_S$ .
- 

$0 < \epsilon, \xi < 1$ . Provided that the constant step size  $\eta > 0$  and the epoch length  $T$  are chosen such that

$$\eta \leq \frac{c_0 \xi^2}{r^2} \delta, \quad T \geq \frac{c_1 \log(2/\xi)}{\eta \delta}, \quad T \eta^2 r^2 + r \eta \sqrt{T \log(2/\xi)} \leq c_2 \quad (11)$$

for certain universal constants  $c_0, c_1, c_2 > 0$ , then successive estimates of VR-OPI (summarized in Algorithm 2) after  $S = \left\lceil \frac{\log(1/\epsilon)}{\log(2/\xi)} \right\rceil$  epochs satisfy

$$|\langle \tilde{\mathbf{u}}_S, \mathbf{v}_1 \rangle|^2 \geq 1 - \epsilon \quad (12)$$

with probability exceeding  $1 - \left\lceil \frac{\log(1/\epsilon)}{\log(2/\xi)} \right\rceil$ . Typical parameter values are  $\eta = 20/m$ ,  $S = 100$ , and  $T = |\bar{\mathcal{I}}_0|$ .

The proof of Proposition 1 can be found in [33]. Even though PCA in (7) is nonconvex, the SGD based VR-OPI algorithm converges to the globally optimal solution under mild conditions [33]. Moreover, fixing any  $\xi \in (0, 1)$ , conditions in (11) hold true when  $T$  is chosen to be on the order of  $1/(\eta \delta)$  and  $\eta$  to be sufficiently smaller than  $\delta/r^2$ . Expressed differently, if VR-OPI runs  $T = \Theta(r^2/\delta^2)$  iterations per epoch for a total number  $S = \Theta(\log(1/\epsilon))$  of epochs, then the returned VR-OPI estimate is  $\epsilon$ -accurate with probability at least  $1 - \lceil \log_2(1/\epsilon) \rceil \xi$ . It is clear also that each epoch takes  $\mathcal{O}(n(T + |\bar{\mathcal{I}}_0|))$  time to implement, thus yielding a total runtime of

$$\mathcal{O}\left(n \left( |\bar{\mathcal{I}}_0| + \frac{r^2}{\delta^2} \right) \log(1/\epsilon) \right) \quad (13)$$

which validates the exponential convergence rate of VR-OPI. In addition, when  $\delta/r \geq \Omega(1/\sqrt{|\bar{\mathcal{I}}_0|})$ , the total runtime reduces to  $\mathcal{O}(n|\bar{\mathcal{I}}_0| \log(1/\epsilon))$  up to log-factors. It is worth emphasizing that the required running time is proportional to the time required to scan the selected data once, which is in stark contrast to the runtime

of  $\mathcal{O}(n|\bar{\mathcal{I}}_0| \log(1/\epsilon)/\delta)$  using power method [32]. Simulated tests in Section 4 corroborate the effectiveness of VR-OPI over the popular power method in processing data involving large dimensions  $m$  and/or  $n$ .

### 2.3 Stochastic Truncated Gradient Stage

Driven by the need of efficiently processing large-scale phaseless data in imaging applications, a stochastic solution algorithm is put forth for minimizing the amplitude-based cost function in (4). To ensure good performance, the gradient regularization rule in (10) is also accounted for to lead to our truncated stochastic gradient iterations. It is worth mentioning that the Kaczmarz method [36] was also used for solving a system of phaseless quadratic equations in [28]. However, the Kaczmarz variants of block or randomized updates converge to at most a neighborhood of the optimal solution  $\mathbf{x}$ . Distance between the Kaczmarz estimates and  $\mathbf{x}$  is bounded in terms of the dimension  $m$  and the size of the amplitude data vector  $\boldsymbol{\psi}$  measured by the  $\ell_1$ - or  $\ell_\infty$ -norm. Nevertheless, the obtained bounds of the form  $m\|\mathbf{y}\|_1$  or  $m\|\mathbf{y}\|_\infty$  are rather loose ( $m$  typically very large) and less attractive than the geometric convergence to the global solution  $\mathbf{x}$  to be established for also stochastic iterations based STAF.

Adopting the intensity-based Poisson likelihood function (3), an incremental version of TWF was developed in [22], which provably converges to  $\mathbf{x}$  in linear time. Albeit achieving improved empirical performance and faster convergence over TWF in terms of the number of passes over the entire data to produce an  $\epsilon$ -accurate solution [13], the number of measurements it requires for exact recovery is still relatively far from the information-theoretic limits. Specifically for the real-valued Gaussian  $\mathbf{a}_i$  designs, ITWF requires about  $m \geq 3.2n$  noiseless measurements to guarantee exact recovery relative to  $4.5n$  for TWF [13]. Recall that TAF achieves exact recovery from about  $3n$  measurements [14]. Furthermore, it has been demonstrated that, contrary to gradient iterations easy to be trapped in saddle points in nonconvex optimization, stochastic iterations are able to escape saddle points and converge globally to at least a local minimum [24]. Hence, besides the appealing computational advantage, stochastic counterparts of TAF may further improve the performance over TAF, as also asserted by the comparison between ITWF and TWF. In the following, we present two STAF variants: Starting with an initial estimate  $\mathbf{z}_0$  found using VR-OPI in Algorithm 2, the first variant successively updates  $\mathbf{z}_0$  via the ordinary amplitude-based stochastic gradient iterations with a constant step size  $\mu > 0$  chosen on the order of  $1/n$ , while the second operates much like the Kaczmarz method, yet both suitably account for the truncation rule in (10).

For simplicity of exposition, let us rewrite the amplitude-based cost function as follows

$$\underset{\mathbf{z} \in \mathbb{R}^n}{\text{minimize}} \quad \ell(\mathbf{z}) = \sum_{i=1}^m \ell_i(\mathbf{z}) := \frac{1}{2} \sum_{i=1}^m (\psi_i - |\mathbf{a}_i^T \mathbf{z}|)^2 \quad (14)$$

where the factor of  $1/2$  is introduced for notational convenience. It is clear that the objective function  $\ell(\mathbf{z})$  or each  $\ell_i(\mathbf{z})$  in (14) is nonconvex and nonsmooth; hence the optimization in (14) is computationally intractable in general [37]. Along the lines of nonconvex paradigms including WF [1], TWF [13], and TAF [14], our approach to solving the problem at hand amounts to iteratively refining the initial estimate  $\mathbf{z}_0$  by means of the truncated stochastic gradient iterations. This is in contrast to TAF relying on (truncated) gradient-type

iterations [14]. STAF processes one datum at a time and evaluates the generalized gradient of one component function  $\ell_{i_t}(\mathbf{z})$  for some index  $i_t \in \{1, 2, \dots, m\}$  per iteration  $t \geq 0$ . Precisely, STAF successively updates  $\mathbf{z}_0$  using the following truncated stochastic gradient iterations

$$\mathbf{z}_{t+1} = \mathbf{z}_t - \mu_t \partial \ell_{i_t}(\mathbf{z}_t) \mathbb{1}_{\{|\mathbf{a}_{i_t}^\mathcal{T} \mathbf{z}_t| / |\mathbf{a}_{i_t}^\mathcal{T} \mathbf{x}| \geq 1/(1+\gamma)\}}, \quad t = 0, 1, \dots \quad (15)$$

with

$$\partial \ell_{i_t}(\mathbf{z}_t) = \left( \mathbf{a}_{i_t}^\mathcal{T} \mathbf{z}_t - \psi_{i_t} \frac{\mathbf{a}_{i_t}^\mathcal{T} \mathbf{z}_t}{|\mathbf{a}_{i_t}^\mathcal{T} \mathbf{z}_t|} \right) \mathbf{a}_{i_t} \quad (16)$$

where  $\mu_t$  is either set to be a constant  $\mu > 0$  on the order of  $1/n$ , or taken as the time-varying one in Kaczmarz method  $\mu_t = 1/\|\mathbf{a}_{i_t}\|^2$  [36]. The index  $i_t$  is sampled uniformly at random or with given probabilities from  $[m] = \{1, 2, \dots, m\}$ , or it simply cycles through the entire set  $[m]$ . The term  $\partial \ell_{i_t}(\mathbf{z}_t)$  is a generalized gradient of the nonconvex and nonsmooth function  $\ell_{i_t}(\mathbf{z})$  evaluated at  $\mathbf{z}_t$ , which corresponds to a subgradient in the convex nonsmooth optimization regime. More details regarding the generalized gradient can be found in [38, Definition 1], [14]. In addition, fixing truncation threshold  $\gamma = 0.7$ , the indicator function  $\mathbb{1}_{\{|\mathbf{a}_{i_t}^\mathcal{T} \mathbf{z}_t| / |\mathbf{a}_{i_t}^\mathcal{T} \mathbf{x}| \geq 1/(1+\gamma)\}}$  in (15) takes 1 if  $|\mathbf{a}_{i_t}^\mathcal{T} \mathbf{z}_t| / |\mathbf{a}_{i_t}^\mathcal{T} \mathbf{x}| \geq 1/(1+\gamma)$  holds true; and 0 otherwise. It is worth stressing that this truncation rule provably rejects ‘bad’ search directions with high probability. Although in the context of large-scale linear regressions, similar ideas such as censoring have been advocated for speeding up the SGD-type algorithms [39], [40]. Numerical tests demonstrating the performance improvement using the stochastic truncated iterations will be presented in Section 4.

---

**Algorithm 3** Stochastic truncated amplitude flow (STAF) algorithm

---

- 1: **Input:** Sampling vectors  $\{\mathbf{a}_i\}_{i=1}^m$ , and data  $\{\psi_i := |\langle \mathbf{a}_i, \mathbf{x} \rangle|\}_{i=1}^m$ ; the maximum number of iterations  $T = 500m$ ; by default, take constant step sizes  $\mu = 0.8/n$  or  $\mu = 1.2/n$  in the real- or complex-valued Gaussian models, truncation thresholds  $|\bar{\mathcal{I}}_0| = \lceil \frac{1}{6}m \rceil$ , and  $\gamma = 0.7$ .
- 2: **Evaluate**  $\bar{\mathcal{I}}_0$  to consist of indices associated with the  $|\bar{\mathcal{I}}_0|$  largest values among  $\{\psi_i / \|\mathbf{a}_i\|\}$ .
- 3: **Initialize**  $\mathbf{z}_0$  as  $\sqrt{\frac{1}{m} \sum_{i=1}^m \psi_i^2} \tilde{\mathbf{z}}_0$ , where  $\tilde{\mathbf{z}}_0$  is obtained via Algorithm 2 with  $\bar{\mathbf{Y}}_0 := \frac{1}{|\bar{\mathcal{I}}_0|} \sum_{i \in \bar{\mathcal{I}}_0} \frac{\mathbf{a}_i \mathbf{a}_i^\mathcal{T}}{\|\mathbf{a}_i\|^2}$ .
- 4: **For**  $t = 0$  **to**  $T - 1$  **do**

$$\mathbf{z}_{t+1} = \mathbf{z}_t - \mu \left( \mathbf{a}_{i_t}^\mathcal{T} \mathbf{z}_t - \psi_{i_t} \frac{\mathbf{a}_{i_t}^\mathcal{T} \mathbf{z}_t}{|\mathbf{a}_{i_t}^\mathcal{T} \mathbf{z}_t|} \right) \mathbf{a}_{i_t} \mathbb{1}_{\{|\mathbf{a}_{i_t}^\mathcal{T} \mathbf{z}_t| \geq \frac{1}{1+\gamma} \psi_{i_t}\}} \quad (17)$$

where  $i_t$  is sampled uniformly at random from  $[m] = \{1, 2, \dots, m\}$ , or,

$$\mathbf{z}_{t+1} = \mathbf{z}_t - \frac{1}{\|\mathbf{a}_{i_t}\|^2} \left( \mathbf{a}_{i_t}^\mathcal{T} \mathbf{z}_t - \psi_{i_t} \frac{\mathbf{a}_{i_t}^\mathcal{T} \mathbf{z}_t}{|\mathbf{a}_{i_t}^\mathcal{T} \mathbf{z}_t|} \right) \mathbf{a}_{i_t} \mathbb{1}_{\{|\mathbf{a}_{i_t}^\mathcal{T} \mathbf{z}_t| \geq \frac{1}{1+\gamma} \psi_{i_t}\}} \quad (18)$$

where  $i_t$  is sampled at random from  $[m]$  with probability proportional to  $\|\mathbf{a}_{i_t}\|^2$ .

- 5: **End For**
  - 6: **Output:**  $\mathbf{z}_T$ .
-

### 3 Main Results

The proposed STAF scheme is summarized in Algorithm 3, in which either the constant step size  $\mu$ -based truncated stochastic gradient iterations in (17), or the truncated Kaczmarz iterations in (18) can be selected. Armed with an initialization obtained using VR-OPI, both STAF variants will be shown to converge at an exponential rate to the globally optimal solution with high probability, as soon as the ratio  $m/n$  exceeds some numerical constant.

Assuming a number  $m$  of independent data samples  $\{(\mathbf{a}_i; \psi_i)\}$  drawn from the real-valued Gaussian model, the following theorem establishes theoretical performance of STAF in the absence of noise.

**Theorem 1 (Exact recovery).** *Consider the noiseless measurements  $\psi_i = |\mathbf{a}_i^\top \mathbf{x}|$  with an arbitrary signal  $\mathbf{x} \in \mathbb{R}^n$ , where i.i.d.  $\mathbf{a}_i \sim \mathcal{N}(\mathbf{0}, \mathbf{I}_n)$ ,  $1 \leq i \leq m$ . Suppose the step size  $\mu_t$  is either set to be a constant  $\mu > 0$  as per (17), or chosen to be the Kaczmarz one  $1/\|\mathbf{a}_{i_t}\|^2$  as per (18) with the corresponding index sampling scheme. If the following hold true*

$$m \geq c_0 n \quad \text{and} \quad \mu \leq \mu_0/n, \quad (19)$$

*then with probability at least  $1 - c_1 m \exp(-c_2 n)$ , the stochastic truncated amplitude flow (STAF) estimates (tabulated in Algorithm 3 with default parameters) satisfy*

$$\mathbb{E}_{\mathcal{P}_t} [\text{dist}^2(\mathbf{z}_t, \mathbf{x})] \leq \rho \left(1 - \frac{\nu}{n}\right)^t \|\mathbf{x}\|^2, \quad t = 0, 1, \dots \quad (20)$$

*for  $\rho = 1/10$  as well as some numerical constant  $\nu > 0$ , where the expectation is taken over the path sequence  $\mathcal{P}_t := \{i_0, i_1, \dots, i_{t-1}\}$ , and  $c_0, c_1, c_2, \mu_0 > 0$  are certain universal constants.*

The proof of Theorem 1 is deferred to Section 5. Apparently, the mean-square distance between the iterate and the global solution is reduced by a factor of  $(1 - \nu/n)^m$  after one pass through the entire data. Heed that the expectation  $\mathbb{E}_{\mathcal{P}_t}[\cdot]$  in (20) is taken over the algorithmic randomness  $\mathcal{P}_t$  rather than over the data. This is important since in general the data may be given as is and deterministic. Although only performing stochastic iterations in (17) and (18), STAF still enjoys a linear convergence rate. This is in contrast to typical SGD methods, where variance reduction techniques controlling the variance of the stochastic gradients are required to achieve a linear convergence rate [35, 33], as was done in Algorithm 2. Moreover, the largest constant step size that STAF can afford is estimated to be  $\mu_0 = 0.8469$ , giving rise to a convergence factor of  $\nu_0 = 0.0696$  in (20). When truncated Kaczmarz iterations are implemented,  $\nu$  is estimated to be 1.0091 much larger than the one in the constant step size case. Our observations from numerical experiments also confirm that the Kaczmarz-based STAF in (18) converges faster than the constant step-size based one in (17), yet it is slightly more sensitive to the noisy data.

### 4 Simulated Tests

In this section, extensive numerical experiments evaluating performance of STAF using both synthetic data and real images are presented. STAF was thoroughly compared with the existing alternatives including

TAF [14], (T)WF [1, 13], and ITWF [22]. For fair comparisons, all the parameters pertinent to implementation of each algorithm were set to their suggested values. The initialization in each scheme was found based on a number of (power/stochastic) iterations equivalent to 100 passes over the entire data, which was subsequently refined by number of iterations equivalent to 1,000 passes; unless otherwise stated. Simulated estimates were averaged over 100 independent Monte Carlo trials without stressing this explicitly each time. Two performance evaluation metrics were used: the relative root mean-square error defined as  $\text{Relative error} := \text{dist}(\mathbf{z}, \mathbf{x})/\|\mathbf{x}\|$ ; and the empirical successful recovery rate among 100 independent runs, in which a success is declared when the returned estimate incurs a relative error less than  $10^{-5}$  [1]. Tests using both noiseless/noisy real-/complex-valued Gaussian models  $\psi_i = |\mathbf{a}_i^H \mathbf{x}| + \eta_i$  were conducted, where the i.i.d. noise obeys  $\eta_i \sim \mathcal{N}(0, \sigma^2 \|\mathbf{x}\|^2)$ . The Matlab implementations of STAF can be downloaded from <http://www.tc.umn.edu/~gangwang/TAF>.

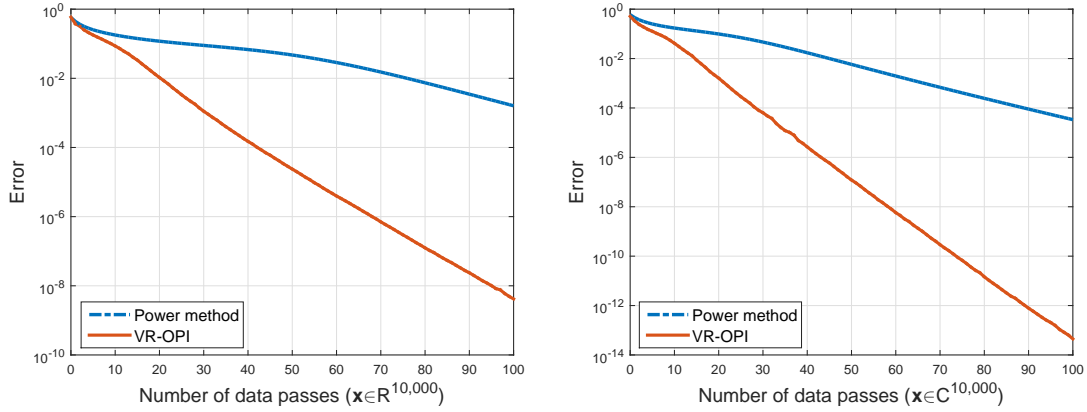


Figure 2: The error evolution of the iterates using: i) power method in Algorithm 1; and iii) the developed VR-OPI in Algorithm 2 for solve the orthogonality-promoting initialization problem in (7) with step size  $\eta = 1$ . Left: The noiseless real-valued Gaussian model with  $\mathbf{x} \sim \mathcal{N}(\mathbf{0}, \mathbf{I}_n)$ ,  $\mathbf{a}_i \sim \mathcal{N}(\mathbf{0}, \mathbf{I}_n)$ , where  $n = 10^4$ , and  $m = 2n - 1$ . Right: The noiseless complex-valued Gaussian model with  $\mathbf{x} \sim \mathcal{CN}(\mathbf{0}, \mathbf{I}_n)$ ,  $\mathbf{a}_i \sim \mathcal{CN}(\mathbf{0}, \mathbf{I}_n)$ , where  $n = 10^4$ , and  $m = 4n - 4$ .

The first experiment compares VR-OPI in Algorithm 2 and power method in Algorithm 1 to solve the orthogonality-promoting initialization optimization in (7). The comparison is carried out in terms of the number of data passes to achieve the same solution accuracy, in which one pass through the selected data amounts to a number  $|\bar{\mathcal{I}}_0|$  of gradient evaluations of component functions. First, synthetic data based experiments are conducted using the real-/complex-valued Gaussian models with  $n = 10,000$  under the known sufficient conditions for uniqueness, i.e.,  $m = 2n - 1$  in the real case, and  $m = 4n - 4$  in the complex case. Figure 2 plots the error evolution of the iterates  $\mathbf{u}_t$  in power method and VR-OPI, where the error in logarithmic scale is defined as  $\log_{10} \left( 1 - \frac{\|D^T \mathbf{u}_t\|^2}{\|D^T \mathbf{v}_0\|^2} \right)$  with the exact principal eigenvector  $\mathbf{v}_0$  computed

from the SVD of  $\bar{Y}_0 = DD^T$  in (7). Apparently, the cheap stochastic iterations based VR-OPI algorithm achieves certain solution accuracy within considerably fewer gradient evaluations or data passes in both real and complex cases. This is significant for tasks of large  $|\bar{\mathcal{I}}_0|$ , or equivalently large dimension  $m$  (due to  $|\bar{\mathcal{I}}_0| = 5m/6$  by default), since one less data pass implies  $|\bar{\mathcal{I}}_0|$  fewer gradient evaluations and thus saves a sizable amount of computational resources.

The second experiment evaluates the *second* (i.e., refinement) stage of STAF relative to its competing alternatives including those of (T)WF, TAF, and ITWF in a variety of settings. In this experiment, for fairness, all schemes were initialized using the *same* orthogonality-promoting initialization found using 100 power iterations, and subsequently applied a number of iterations equivalent to  $T = 1,000$  data passes. First, tests on the noiseless real- and complex-valued Gaussian models were conducted, where i.i.d.  $\mathbf{a}_i \in \mathbb{R}^{1,000} \sim \mathcal{N}(\mathbf{0}, \mathbf{I}_{1,000})$ ,  $\mathbf{x} \in \mathbb{R}^{1,000} \sim \mathcal{N}(\mathbf{0}, \mathbf{I}_{1,000})$ , and i.i.d.  $\mathbf{a}_i \in \mathbb{C}^{1,000} \sim \mathcal{CN}(\mathbf{0}, \mathbf{I}_{1,000})$ ,  $\mathbf{x} \in \mathbb{C}^{1,000} \sim \mathcal{CN}(\mathbf{0}, \mathbf{I}_{1,000})$ , respectively. Figure 3 presents the empirical success rate of all considered schemes with  $m/n$  varying by 0.1 from 1 to 7. Figure 4 compares the convergence speed of various schemes in terms of the number of data passes to produce solutions of a given accuracy. Apparently, starting with the same initialization, STAF outperforms its competing alternatives under both real-/complex-valued Gaussian models. In particular, SGD-based STAF improves in terms of exact recovery and convergence speed over the state-of-the-art gradient-type TAF, corroborating the promising benefit of using SGD-type solution algorithms in escaping saddle points of nonconvex optimization [24, 22].

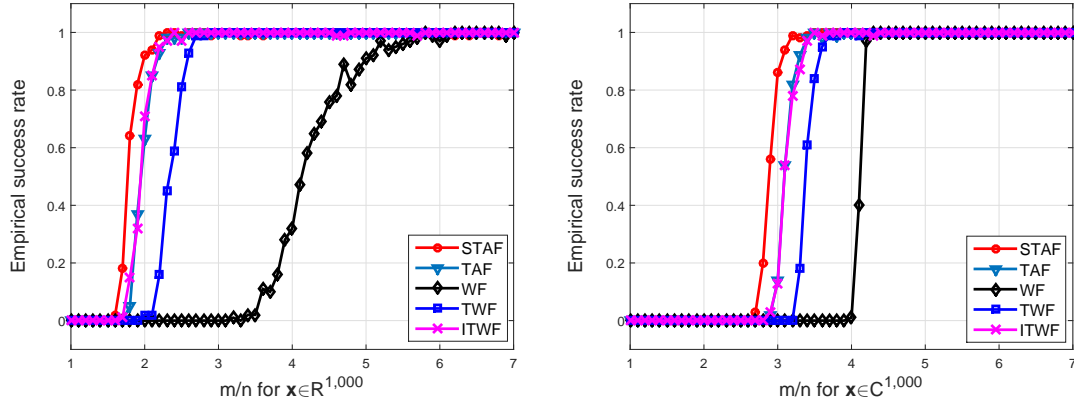


Figure 3: Empirical success rate for: i) WF [1]; ii) TWF [13]; iii) ITAF [22]; iv) TAF [14]; and v) STAF with  $n = 1,000$  and  $m/n$  varying by 0.1 from 1 to 7 under the *same* orthogonality-promoting initialization. Left: The noiseless real-valued Gaussian model with  $\mathbf{x} \sim \mathcal{N}(\mathbf{0}, \mathbf{I}_n)$  and  $\mathbf{a}_i \sim \mathcal{N}(\mathbf{0}, \mathbf{I}_n)$ ; Right: The noiseless complex-valued Gaussian model with  $\mathbf{x} \sim \mathcal{CN}(\mathbf{0}, \mathbf{I}_n)$  and  $\mathbf{a}_i \sim \mathcal{CN}(\mathbf{0}, \mathbf{I}_n)$ .

The previous experiment showed improved performance of STAF over its competing alternatives under the same initialization. Now, we present numerical results comparing different schemes with their own initialization, namely, WF with spectral initialization [1], (I)TWF with truncated spectral initialization [13],

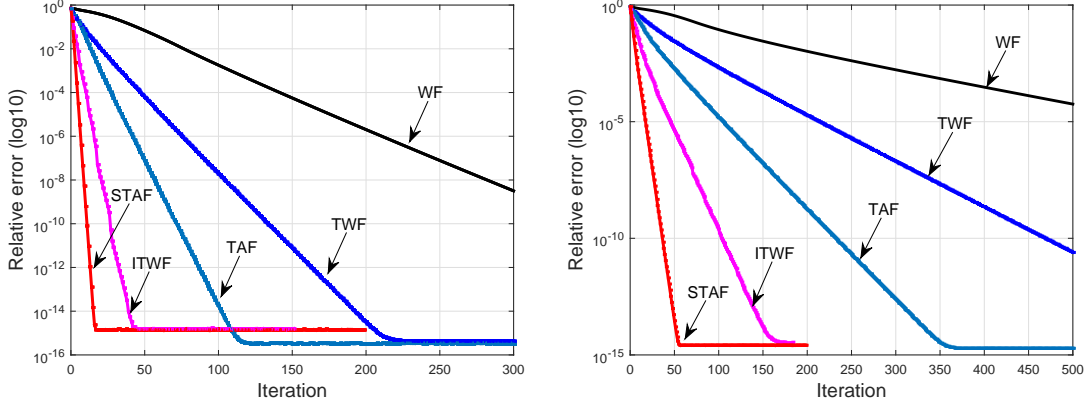


Figure 4: The relative error versus iteration using: i) WF [1]; ii) TWF [13]; iii) ITAF [22]; iv) TAF [14]; and v) STAF under the *same* orthogonality-promoting initialization. Left: The noiseless real-valued Gaussian model with  $\mathbf{x} \sim \mathcal{N}(\mathbf{0}, \mathbf{I}_n)$  and  $\mathbf{a}_i \sim \mathcal{N}(\mathbf{0}, \mathbf{I}_n)$ ; Right: The noiseless complex-valued Gaussian model with  $\mathbf{x} \sim \mathcal{CN}(\mathbf{0}, \mathbf{I}_n)$  and  $\mathbf{a}_i \sim \mathcal{CN}(\mathbf{0}, \mathbf{I}_n)$ , where  $n = 1,000$ , and  $m = 5n$ .

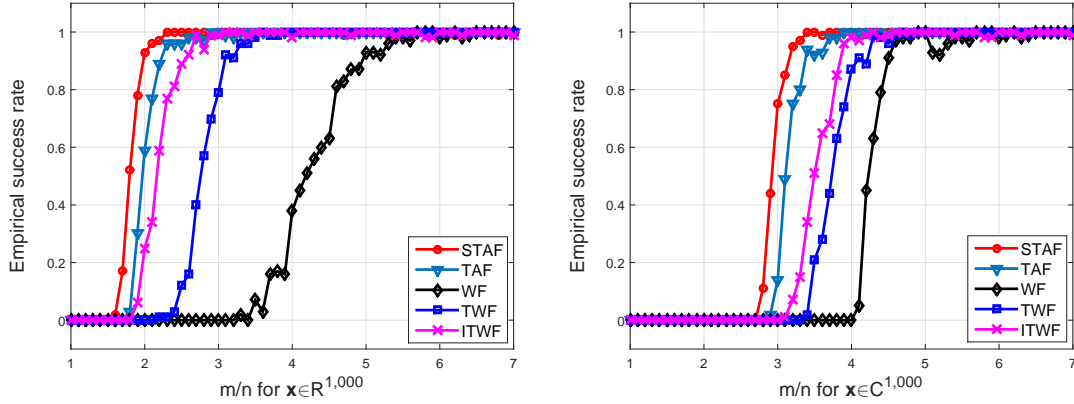


Figure 5: Empirical success rate for: i) WF [1]; ii) TWF [13]; iii) ITAF [22]; iv) TAF [14]; and v) STAF with  $n = 1,000$  and  $m/n$  varying 0.1 from 1 to 7. Left: The noiseless real-valued Gaussian model with  $\mathbf{x} \sim \mathcal{N}(\mathbf{0}, \mathbf{I}_n)$  and  $\mathbf{a}_i \sim \mathcal{N}(\mathbf{0}, \mathbf{I}_n)$ ; Right: The noiseless complex-valued Gaussian model with  $\mathbf{x} \sim \mathcal{CN}(\mathbf{0}, \mathbf{I}_n)$  and  $\mathbf{a}_i \sim \mathcal{CN}(\mathbf{0}, \mathbf{I}_n)$ .

as well as TAF with orthogonality-promoting initialization using power iterations [14] and STAF with variance-reduced orthogonality-promoting initialization.

To demonstrate the robustness of STAF against the noise, we perform stable phase retrieval under the noisy real-/complex-valued Gaussian model  $\psi_i = |\mathbf{a}_i^H \mathbf{x}| + \eta_i$ , where i.i.d.  $\eta_i \sim \mathcal{N}(\mathbf{0}, \sigma^2 \mathbf{I})$  with  $\sigma^2 = 0.1^2 \|\mathbf{x}\|^2$ .

Curves in Fig. 6 clearly shows near-perfect statistical performance and fast convergence of STAF.

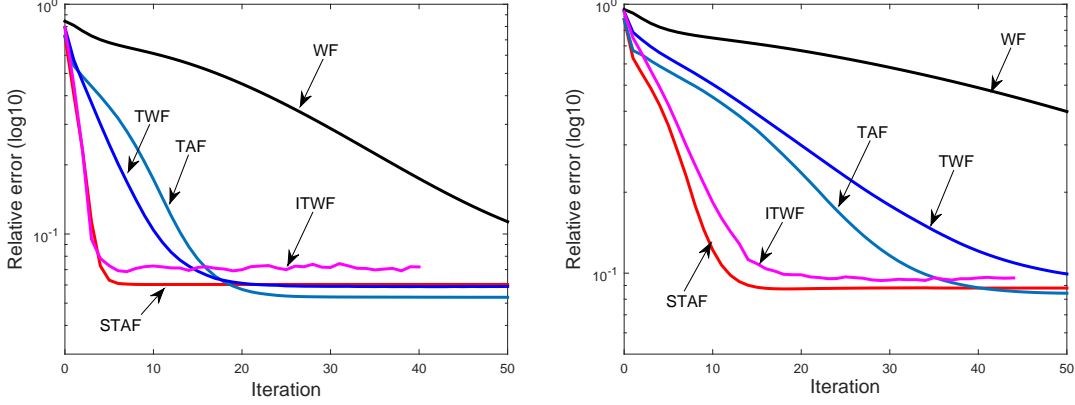


Figure 6: The relative error versus iteration using: i) WF [1]; ii) TWF [13]; iii) ITAF [22]; iv) TAF [14]; and v) STAF with  $n = 1,000$  and  $m/n = 5$ . Left: The noisy real-valued Gaussian model with  $\mathbf{x} \sim \mathcal{N}(\mathbf{0}, \mathbf{I}_n)$  and  $\mathbf{a}_i \sim \mathcal{N}(\mathbf{0}, \mathbf{I}_n)$ ; Right: The noisy complex-valued Gaussian model with  $\mathbf{x} \sim \mathcal{CN}(\mathbf{0}, \mathbf{I}_n)$  and  $\mathbf{a}_i \sim \mathcal{CN}(\mathbf{0}, \mathbf{I}_n)$ .

Finally, to demonstrate the effectiveness and scalability of STAF on real data, the Milky Way Galaxy image<sup>1</sup> is involved. The colorful image of RGB bands is denoted by  $\mathbf{X} \in \mathbb{R}^{1080 \times 1920 \times 3}$ , in which the first two indices encode the pixel location, and the third the color band. The algorithm was run independently on each of the three RGB images. Consider the physically realizable measurements called coded diffraction patterns (CDP) using random masks [12, 1, 13]. Letting  $\mathbf{x} \in \mathbb{R}^n$  be a vectorization of a certain band of  $\mathbf{X}$ , then one has magnitude-only measurements of the form

$$\psi^{(k)} = |\mathbf{F}\mathbf{D}^{(k)}\mathbf{x}|, \quad 1 \leq k \leq K, \quad (21)$$

where  $n = 1,080 \times 1,920 = 2,073,600$ ,  $\mathbf{F}$  is an  $n \times n$  discrete Fourier transform matrix, and  $\mathbf{D}^{(k)}$  is a diagonal matrix whose diagonal entries are sampled uniformly at random from phase delays  $\{1, -1, j, -j\}$ , with  $j$  denoting the imaginary unit. A number  $K = 8$  of random masks were employed to generate CDP measurements, thus rendering a total number  $m = nK$  of quadratic measurements. In this part, since the fast Fourier transform (FFT) can be implemented in  $\mathcal{O}(n \log n)$  instead of  $\mathcal{O}(n^2)$  time, the advantage of using STAF of optimal iteration complexity is less significant. Hence, instead of processing one quadratic measurement per iteration, a block STAF version processes per iteration  $n^2$  measurements associated with one random mask. That is, STAF samples randomly the index  $k \in \{1, 2, \dots, K\}$  of masks in (21), and updates the iterate using all diffraction patterns corresponding to the  $k$ -th mask. In this case, STAF is able to leverage the efficient implementation of FFT, and it converges quickly. Figure 7 displays the recovered

<sup>1</sup>The Milky Way Galaxy image is downloaded from <http://pics-about-space.com/milky-way-galaxy>.



images, where the top is obtained after 100 data passes of VR-OPI iterations, and the bottom is produced by 100 data passes of STAF iterations refining the initialization. Apparently, the recovered images corroborate effectiveness of STAF in real-world conditions.



Figure 7: The recovered images after: the variance-reduced orthogonality-promoting initialization stage (top panel), and the STAF refinement (bottom panel) on the Milky Way Galaxy image using  $K = 8$  random masks.

## 5 Proof for Theorem 1

Recall from Theorem 1 in [14] that when  $m/n$  exceeds some universal constant  $c_0 > 0$ , the estimate  $\mathbf{z}_0$  returned by the orthogonality-promoting initialization method obeys

$$\text{dist}(\mathbf{z}_0, \mathbf{x}) \leq \rho \|\mathbf{x}\| \quad (22)$$

with high probability for any sufficiently small constant  $\rho > 0$ . Take without loss of generality that  $\rho = 1/10$  next. Along the lines of (T)WF and TAF, to prove Theorem 1, it suffices to show that successive STAF iterates  $\mathbf{z}_t$  are on average locally contractive around the planted solution  $\mathbf{x}$ , as asserted in the following proposition.

**Proposition 2 (Local error contraction).** *Consider the noiseless measurements  $\psi_i = |\mathbf{a}_i^\top \mathbf{x}|$  with an arbitrary signal  $\mathbf{x} \in \mathbb{R}^n$ , and i.i.d.  $\mathbf{a}_i \sim \mathcal{N}(\mathbf{0}, \mathbf{I}_n)$ ,  $1 \leq i \leq m$ . Under the default algorithmic parameters given in Algorithm 3, there exist universal constants  $c_0, c_1, c_2 > 0$ , and  $\nu > 0$ , such that with probability at least  $1 - c_2 m \exp(-c_1 n)$ , the following holds*

$$\mathbb{E}_{i_t} [\text{dist}^2(\mathbf{z}_{t+1}, \mathbf{x})] \leq \left(1 - \frac{\nu}{n}\right) \text{dist}^2(\mathbf{z}_t, \mathbf{x}), \quad t = 0, 1, \dots \quad (23)$$

*simultaneously for all  $\mathbf{z}_t \in \mathbb{R}^n$  satisfying (22), provided that  $m \geq c_0 n$ .*

The proof of Proposition 2 is relegated to Appendix 6. Proposition 2 demonstrates the monotonic decrease of the mean-square estimation error: Once entering a reasonably small-size neighborhood of  $\mathbf{x}$ , successive iterates of STAF will be attracted toward  $\mathbf{x}$  at a geometric rate. Upon establishing the local error contraction property in (23), take expectation of both sides in (23) over  $i_{t-1}$ , and apply Proposition (23) again to yield a similar relation for the previous iteration. Continuing this process to reach the initialization  $\mathbf{z}_0$  and appealing to the initialization result in (22) collectively lead to (20), hence concluding the proof of Theorem 1.

## 6 Concluding Remarks

This paper developed a new linear-time algorithm called STAF to solve systems of phaseless quadratic equations, which builds on but considerably broadens the scope of the state-of-the-art TAF algorithm [14]. Adopting the amplitude-based nonconvex formulation, STAF is a two-stage iterative solution algorithm. It consists of first obtaining an orthogonality-promoting initialization using a variance-reduced stochastic optimization algorithm, and subsequently refining the initial estimate via truncated stochastic amplitude-based iterations. STAF was shown to be able to recover any signal from about as many equations as unknowns. In contrast to existing alternatives, both stages of STAF achieve optimal iteration and computational complexities suitable for large-scale implementations. Numerical tests involving synthetic data and real images corroborate the advantages of STAF in terms of both exact recovery performance and convergence speed over the state-of-the-art algorithms including TAF, (T)WF, and ITWF.

A few pertinent future research directions include exploiting the possibility of orthogonality-promoting initialization in the context of robust phase retrieval and faster semidefinite optimization, and developing suitable gradient regularization rules for general nonconvex optimization tasks. Devising cheap stochastic iterations based iterative solution algorithms for more general convex/nonconvex optimization problems constitutes another meaningful direction.

## Appendix

### Proof of Proposition 2

To prove Proposition 2, let us first define the truncated gradient of  $\ell(\mathbf{z})$  in (14) as follows

$$\nabla \ell_{\text{tr}}(\mathbf{z}) = \sum_{i=1}^m \left( \mathbf{a}_i^T \mathbf{z} - \psi_i \frac{\mathbf{a}_i^T \mathbf{z}}{|\mathbf{a}_i^T \mathbf{z}|} \right) \mathbf{a}_i \mathbb{1}_{\{|\mathbf{a}_i^T \mathbf{z}| \geq \frac{1}{1+\gamma} \psi_i\}} \quad (24)$$

which corresponds to the truncated gradient employed in TAF [14]. Instrumental in proving the local error contraction in Proposition 2, the following lemma adopts a sufficient decrease result in [14, Proposition 3]. The sufficient decrease is a key step in establishing the local regularity condition [1, 13, 14], which suffices to prove linear convergence of iterative optimization algorithms.

**Proposition 3.** [14, Proposition 3] *Consider the noise-free measurements  $\psi_i = |\mathbf{a}_i^T \mathbf{x}|$  with i.i.d.  $\mathbf{a}_i \sim \mathcal{N}(\mathbf{0}, \mathbf{I}_n)$ ,  $1 \leq i \leq m$ , and  $\gamma = 0.7$ . For any fixed  $\epsilon > 0$ , there exist universal constants  $c_0, c_1, c_2 > 0$  such that if  $m > c_0 n$ , then the following holds with probability at least  $1 - c_2 \exp(-c_1 m)$ ,*

$$\left\langle \mathbf{h}, \frac{1}{m} \nabla \ell_{\text{tr}}(\mathbf{z}) \right\rangle \geq 2(1 - \zeta_1 - \zeta_2 - 2\epsilon) \|\mathbf{h}\|^2, \quad \mathbf{h} = \mathbf{z} - \mathbf{x} \quad (25)$$

for all  $\mathbf{x}, \mathbf{z} \in \mathbb{R}^n$  such that  $\|\mathbf{h}\|/\|\mathbf{x}\| \leq \frac{1}{10}$ , where estimates  $\zeta_1 \approx 0.0782$ , and  $\zeta_2 \approx 0.3894$ .

Now let us turn to the term on the left hand side of (23), which after plugging in the update of  $\mathbf{z}_{t+1}$  in (17) or (18) boils down to

$$\begin{aligned} \text{dist}^2(\mathbf{z}_{t+1}, \mathbf{x}) &= \left\| \mathbf{z}_t - \mathbf{x} - \mu_t \left( \mathbf{a}_{i_t}^T \mathbf{z}_t - \psi_{i_t} \frac{\mathbf{a}_{i_t}^T \mathbf{z}_t}{|\mathbf{a}_{i_t}^T \mathbf{z}_t|} \right) \mathbf{a}_{i_t} \mathbb{1}_{\{|\mathbf{a}_{i_t}^T \mathbf{z}_t| \geq \frac{1}{1+\gamma} \psi_{i_t}\}} \right\|^2 \\ &= \|\mathbf{h}_t\|^2 - 2\mu_t \left( \mathbf{a}_{i_t}^T \mathbf{z}_t - \psi_{i_t} \frac{\mathbf{a}_{i_t}^T \mathbf{z}_t}{|\mathbf{a}_{i_t}^T \mathbf{z}_t|} \right) \mathbf{a}_{i_t}^T \mathbf{h}_t \mathbb{1}_{\{|\mathbf{a}_{i_t}^T \mathbf{z}_t| \geq \frac{1}{1+\gamma} \psi_{i_t}\}} \\ &\quad + \mu_t^2 \left( \mathbf{a}_{i_t}^T \mathbf{z}_t - \psi_{i_t} \frac{\mathbf{a}_{i_t}^T \mathbf{z}_t}{|\mathbf{a}_{i_t}^T \mathbf{z}_t|} \right)^2 \|\mathbf{a}_{i_t}\|^2 \mathbb{1}_{\{|\mathbf{a}_{i_t}^T \mathbf{z}_t| \geq \frac{1}{1+\gamma} \psi_{i_t}\}}, \end{aligned} \quad (26)$$

where  $\mu_t = \mu > 0$  with  $i_t \in \{1, 2, \dots, m\}$  sampled uniformly at random in (17), or  $\mu_t = 1/\|\mathbf{a}_{i_t}\|^2$  with  $i_t \in \{1, 2, \dots, m\}$  selected with probability proportional to  $\|\mathbf{a}_{i_t}\|^2$  in (18).

Consider first the constant step size case in (17). Take the expectation of both sides in (26) with respect to the selection of index  $i_t$  (rather than the data randomness) to yield

$$\begin{aligned} \mathbb{E}_{i_t} [\text{dist}^2(\mathbf{z}_{t+1}, \mathbf{x})] &= \|\mathbf{h}_t\|^2 - \frac{2\mu}{m} \sum_{i_t=1}^m \left( \mathbf{a}_{i_t}^T \mathbf{z}_t - \psi_{i_t} \frac{\mathbf{a}_{i_t}^T \mathbf{z}_t}{|\mathbf{a}_{i_t}^T \mathbf{z}_t|} \right) \mathbf{a}_{i_t}^T \mathbf{h}_t \mathbb{1}_{\{|\mathbf{a}_{i_t}^T \mathbf{z}_t| \geq \frac{1}{1+\gamma} \psi_{i_t}\}} \\ &\quad + \frac{\mu^2}{m} \sum_{i_t=1}^m \left( \mathbf{a}_{i_t}^T \mathbf{z}_t - \psi_{i_t} \frac{\mathbf{a}_{i_t}^T \mathbf{z}_t}{|\mathbf{a}_{i_t}^T \mathbf{z}_t|} \right)^2 \|\mathbf{a}_{i_t}\|^2 \mathbb{1}_{\{|\mathbf{a}_{i_t}^T \mathbf{z}_t| \geq \frac{1}{1+\gamma} \psi_{i_t}\}}. \end{aligned} \quad (27)$$

Now the task reduces to upper bounding the terms on the right hand side of (27). Noticing from (24) that by means of  $\nabla \ell_{\text{tr}}(\mathbf{z}_t)$ , the second term in (27) can be re-expressed as follows

$$\begin{aligned} -\frac{2\mu}{m} \sum_{i_t=1}^m \left( \mathbf{a}_{i_t}^\top \mathbf{z}_t - \psi_{i_t} \frac{\mathbf{a}_{i_t}^\top \mathbf{z}_t}{|\mathbf{a}_{i_t}^\top \mathbf{z}_t|} \right) \mathbf{a}_{i_t}^\top \mathbf{h}_t \mathbb{1}_{\{|\mathbf{a}_{i_t}^\top \mathbf{z}_t| \geq \frac{1}{1+\gamma} \psi_{i_t}\}} &= -\frac{2\mu}{m} \langle \nabla \ell_{\text{tr}}(\mathbf{z}_t), \mathbf{h}_t \rangle \\ &\leq -4\mu (1 - \zeta_1 - \zeta_2 - 2\epsilon) \|\mathbf{h}\|^2 \end{aligned} \quad (28)$$

where the inequality follows from Proposition 3. Regarding the last term in (27), since for the i.i.d. real-valued Gaussian  $\mathbf{a}_i$ 's,  $\max_{i_t \in [m]} \|\mathbf{a}_{i_t}\| \leq 2.3n$  holds with probability at least  $1 - me^{-n/2}$  [14], and also  $\mathbb{1}_{\{|\mathbf{a}_{i_t}^\top \mathbf{z}_t| \geq \frac{1}{1+\gamma} \psi_{i_t}\}} \leq 1$ , then the next holds with high probability

$$\begin{aligned} \frac{\mu^2}{m} \sum_{i_t=1}^m \left( \mathbf{a}_{i_t}^\top \mathbf{z}_t - \psi_{i_t} \frac{\mathbf{a}_{i_t}^\top \mathbf{z}_t}{|\mathbf{a}_{i_t}^\top \mathbf{z}_t|} \right)^2 \|\mathbf{a}_{i_t}\|^2 \mathbb{1}_{\{|\mathbf{a}_{i_t}^\top \mathbf{z}_t| \geq \frac{1}{1+\gamma} \psi_{i_t}\}} &\leq \frac{2.3n\mu^2}{m} \sum_{i_t=1}^m (|\mathbf{a}_{i_t}^\top \mathbf{z}_t| - |\mathbf{a}_{i_t}^\top \mathbf{x}|)^2 \\ &\leq \frac{2.3n\mu^2}{m} \sum_{i_t=1}^m (\mathbf{a}_{i_t}^\top \mathbf{z}_t - \mathbf{a}_{i_t}^\top \mathbf{x})^2 \\ &\leq \frac{2.3n\mu^2}{m} \mathbf{h}_t^\top \mathbf{A}^\top \mathbf{A} \mathbf{h}_t \\ &\leq 2.3(1 + \delta)\mu^2 n \|\mathbf{h}_t\|^2, \end{aligned} \quad (29)$$

in which the second inequality comes from  $(|\mathbf{a}_{i_t}^\top \mathbf{z}_t| - |\mathbf{a}_{i_t}^\top \mathbf{x}|)^2 \leq (\mathbf{a}_{i_t}^\top \mathbf{z}_t - \mathbf{a}_{i_t}^\top \mathbf{x})^2$ , and the last inequality arises from the fact that  $\lambda_{\max}(\mathbf{A}^\top \mathbf{A}) \leq (1 + \delta)m$  holds with probability at least  $1 - c'_2 \exp(-c'_1 n \delta^2)$  provided that  $m \geq c'_0 n \delta^{-2}$  for some universal constant  $c'_0, c'_1, c'_2 > 0$  [41, Theorem 5.39].

Substituting (28) and (29) into (27) establishes that

$$\mathbb{E}_{i_t} [\text{dist}^2(\mathbf{z}_{t+1}, \mathbf{x})] \leq [1 - 4\mu (1 - \zeta_1 - \zeta_2 - 2\epsilon) + 2.3(1 + \delta)\mu^2 n] \|\mathbf{h}_t\|^2 \quad (30)$$

holds with probability exceeding  $1 - c_2 m \exp(-c_1 n)$  provided that  $m \geq c_0 n$ , where  $c_0 \geq c'_0 \delta^{-2}$ . To obtain legitimate estimates for the step size, fixing  $\epsilon, \delta > 0$  to be sufficiently small constants, say, e.g., 0.01, then using (30),  $\mu$  can be chosen such that  $4(0.98 - \zeta_1 - \zeta_2) - 2.42\mu n > 0$ , yielding

$$0 < \mu < \frac{4(0.98 - \zeta_1 - \zeta_2)}{2.42n} \approx \frac{0.8469}{n} := \frac{\mu_0}{n}. \quad (31)$$

Plugging  $\mu = c_3/n$  for some  $0 < c_3 \leq \mu_0$  into (30) gives rise to

$$\mathbb{E}_{i_t} [\text{dist}^2(\mathbf{z}_{t+1}, \mathbf{x})] \leq \left(1 - \frac{\nu}{n}\right) \text{dist}^2(\mathbf{z}_t, \mathbf{x}) \quad (32)$$

for  $\nu := 4c_3(1 - \zeta_1 - \zeta_2 - 2\epsilon) - 2.3c_3^2(1 + \delta) \leq \nu_0 := 0.0697$ , where the equality holds at the maximum step size  $\mu = \mu_0$ , hence concluding the proof of Proposition 2 for the constant step size case.

Now let us turn to the case of a time-varying step size, specifically in which  $\mu_t = 1/\|\mathbf{a}_{i_t}\|^2$ , and  $i_t$  is sampled at random from the set  $\{1, 2, \dots, m\}$  with probability  $\|\mathbf{a}_{i_t}\|^2 / \sum_{i_t=1}^m \|\mathbf{a}_{i_t}\|^2 = \|\mathbf{a}_{i_t}\|^2 / \|\mathbf{A}\|_F^2$  [42].

Taking the expectation of both sides in (26) over  $i_t$  gives rise to

$$\begin{aligned}\mathbb{E}_{i_t} [\text{dist}^2(\mathbf{z}_{t+1}, \mathbf{x})] &= \|\mathbf{h}_t\|^2 - 2 \sum_{i_t=1}^m \frac{\|\mathbf{a}_{i_t}\|^2}{\|\mathbf{A}\|_F^2} \frac{1}{\|\mathbf{a}_{i_t}\|^2} \left( \mathbf{a}_{i_t}^\top \mathbf{z}_t - \psi_{i_t} \frac{\mathbf{a}_{i_t}^\top \mathbf{z}_t}{|\mathbf{a}_{i_t}^\top \mathbf{z}_t|} \right) \mathbf{a}_{i_t}^\top \mathbf{h}_t \mathbb{1}_{\{|\mathbf{a}_{i_t}^\top \mathbf{z}_t| \geq \frac{1}{1+\gamma} \psi_{i_t}\}} \\ &\quad + \sum_{i_t=1}^m \frac{\|\mathbf{a}_{i_t}\|^2}{\|\mathbf{A}\|_F^2} \frac{1}{\|\mathbf{a}_{i_t}\|^2} \left( \mathbf{a}_{i_t}^\top \mathbf{z}_t - \psi_{i_t} \frac{\mathbf{a}_{i_t}^\top \mathbf{z}_t}{|\mathbf{a}_{i_t}^\top \mathbf{z}_t|} \right)^2 \mathbb{1}_{\{|\mathbf{a}_{i_t}^\top \mathbf{z}_t| \geq \frac{1}{1+\gamma} \psi_{i_t}\}}.\end{aligned}\quad (33)$$

Consider random  $\mathbf{A} = [\mathbf{a}_1 \dots \mathbf{a}_m]^\top$  with i.i.d. rows  $\mathbf{a}_i \sim \mathcal{N}(\mathbf{0}, \mathbf{I}_n)$  and any fixed  $\sigma > 0$ . Then, by means of Bernstein-type inequality [41, Proposition 5.16],  $|\frac{1}{mn} \|\mathbf{A}\|_F^2 - 1| = |\frac{1}{mn} \sum_{i,j} a_{i,j}^2 - 1| \leq \sigma$  holds with probability at least  $1 - 2 \exp(-mn\sigma^2/8)$ . Therefore, the second term on the right hand side of (33) can be bounded as follows

$$\begin{aligned}& - \frac{2}{\|\mathbf{A}\|_F^2} \sum_{i_t=1}^m \left( \mathbf{a}_{i_t}^\top \mathbf{z}_t - \psi_{i_t} \frac{\mathbf{a}_{i_t}^\top \mathbf{z}_t}{|\mathbf{a}_{i_t}^\top \mathbf{z}_t|} \right) \mathbf{a}_{i_t}^\top \mathbf{h}_t \mathbb{1}_{\{|\mathbf{a}_{i_t}^\top \mathbf{z}_t| \geq \frac{1}{1+\gamma} \psi_{i_t}\}} \\ & \leq - \frac{2}{(1+\sigma)mn} \sum_{i_t=1}^m \left( \mathbf{a}_{i_t}^\top \mathbf{z}_t - \psi_{i_t} \frac{\mathbf{a}_{i_t}^\top \mathbf{z}_t}{|\mathbf{a}_{i_t}^\top \mathbf{z}_t|} \right) \mathbf{a}_{i_t}^\top \mathbf{h}_t \mathbb{1}_{\{|\mathbf{a}_{i_t}^\top \mathbf{z}_t| \geq \frac{1}{1+\gamma} \psi_{i_t}\}} \\ & \leq - \frac{4m}{(1+\sigma)mn} (1 - \zeta_1 - \zeta_2 - 2\epsilon) \|\mathbf{h}\|^2 \\ & \leq - \frac{4}{(1+\sigma)n} (1 - \zeta_1 - \zeta_2 - 2\epsilon) \|\mathbf{h}\|^2\end{aligned}\quad (34)$$

in which the second inequality follows from Proposition 3, and the last inequality from the fact that  $m \geq c_0 n$ . Concerning the last term on the right hand side of (33), one obtains that

$$\begin{aligned}& \sum_{i_t=1}^m \frac{\|\mathbf{a}_{i_t}\|^2}{\|\mathbf{A}\|_F^2} \frac{1}{\|\mathbf{a}_{i_t}\|^2} \left( \mathbf{a}_{i_t}^\top \mathbf{z}_t - \psi_{i_t} \frac{\mathbf{a}_{i_t}^\top \mathbf{z}_t}{|\mathbf{a}_{i_t}^\top \mathbf{z}_t|} \right)^2 \mathbb{1}_{\{|\mathbf{a}_{i_t}^\top \mathbf{z}_t| \geq \frac{1}{1+\gamma} \psi_{i_t}\}} \\ & = \frac{1}{\|\mathbf{A}\|_F^2} \sum_{i_t=1}^m (|\mathbf{a}_{i_t}^\top \mathbf{z}_t| - |\mathbf{a}_{i_t}^\top \mathbf{x}|)^2 \mathbb{1}_{\{|\mathbf{a}_{i_t}^\top \mathbf{z}_t| \geq \frac{1}{1+\gamma} \psi_{i_t}\}} \\ & \leq \frac{1}{\|\mathbf{A}\|_F^2} \sum_{i_t=1}^m (\mathbf{a}_{i_t}^\top \mathbf{z}_t - \mathbf{a}_{i_t}^\top \mathbf{x})^2 \\ & \leq \frac{1}{\|\mathbf{A}\|_F^2} \mathbf{h}_t^\top \mathbf{A}^\top \mathbf{A} \mathbf{h}_t \\ & \leq \frac{(1+\delta)m}{(1-\sigma)mn} \|\mathbf{h}_t\|^2 \\ & \leq \frac{(1+\delta)}{(1-\sigma)n} \|\mathbf{h}_t\|^2,\end{aligned}\quad (35)$$

which holds with high probability as soon as  $m \geq c_0 n \geq c'_0 \delta^{-2} n$ .

Putting results in (33), (34), and (35) together, one establishes that the following holds

$$\mathbb{E}_{i_t} [\text{dist}^2(\mathbf{z}_{t+1}, \mathbf{x})] \leq \left[ 1 - \frac{4}{(1+\sigma)n} (1 - \zeta_1 - \zeta_2 - 2\epsilon) + \frac{(1+\delta)}{(1-\sigma)n} \right] \|\mathbf{h}_t\|^2 \quad (36)$$

with probability at least  $1 - c_2 m \exp(-c_1 n)$  provided that  $m \geq c_0 n$ . Hence, one can set in this case

$$\nu := \frac{4}{(1 + \sigma)n} (1 - \zeta_1 - \zeta_2 - 2\epsilon) - \frac{(1 + \delta)}{(1 - \sigma)n}.$$

Taking without loss of generality  $\delta, \sigma, \epsilon$  to be 0.01, and substituting the estimates of  $\zeta_1, \zeta_2$  into (36), one arrives at  $\nu = 1.0091$  to yield

$$\mathbb{E}_{i_t} [\text{dist}^2(\mathbf{z}_{t+1}, \mathbf{x})] \leq \left(1 - \frac{1.0091}{n}\right) \text{dist}^2(\mathbf{z}_t, \mathbf{x}), \quad (37)$$

which holds with high probability as soon as  $m \geq c_0 n$ , establishing the local error contraction property of the truncated Kaczmarz iterations in (18), as claimed in Proposition 2.

Combining the results in (32) and (37), we proved the local error contraction property claimed in Proposition 2 of the two STAF variants under both the constant and time-varying step sizes.

## References

- [1] E. J. Candès, X. Li, and M. Soltanolkotabi, “Phase retrieval via Wirtinger flow: Theory and algorithms,” *IEEE Trans. Inf. Theory*, vol. 61, no. 4, pp. 1985–2007, Apr. 2015.
- [2] J. Miao, P. Charalambous, J. Kirz, and D. Sayre, “Extending the methodology of X-ray crystallography to allow imaging of micrometre-sized non-crystalline specimens,” *Nature*, vol. 400, no. 6742, pp. 342–344, July 1999.
- [3] R. P. Millane, “Phase retrieval in crystallography and optics,” *J. Opt. Soc. Am. A*, vol. 7, no. 3, pp. 394–411, 1990.
- [4] O. Bunk, A. Diaz, F. Pfeiffer, C. David, B. Schmitt, D. K. Satapathy, and J. F. van der Veen, “Diffractive imaging for periodic samples: Retrieving one-dimensional concentration profiles across microfluidic channels,” *Acta. Crystallogr. A. Found. Crystallogr.*, vol. 63, no. 4, pp. 306–314, 2007.
- [5] K. Jaganathan, Y. C. Eldar, and B. Hassibi, “Phase retrieval: An overview of recent developments,” *arXiv:1510.07713*, 2015.
- [6] E. Hofstetter, “Construction of time-limited functions with specified autocorrelation functions,” *IEEE Trans. Inf. Theory*, vol. 10, no. 2, pp. 119–126, Apr. 1964.
- [7] Y. Shechtman, A. Beck, and Y. C. Eldar, “GESPAR: Efficient phase retrieval of sparse signals,” vol. 62, no. 4, pp. 928–938, Feb. 2014.
- [8] J. R. Fienup, “Phase retrieval algorithms: A comparison,” *Appl. Opt.*, vol. 21, no. 15, pp. 2758–2769, Aug. 1982.

- [9] P. Netrapalli, P. Jain, and S. Sanghavi, “Phase retrieval using alternating minimization,” in *Adv. Neural Inf. Process. Syst.*, Stateline, NV, 2013, pp. 2796–2804.
- [10] C. Qian, X. Fu, N. D. Sidiropoulos, L. Huang, and J. Xie, “Inexact alternating optimization for phase retrieval in the presence of outliers,” *arXiv:1605.00973v1*, 2016.
- [11] G. Wang, G. B. Giannakis, J. Chen, and M. Akçakaya, “SPARTAF: Sparse phase retrieval via truncated amplitude flow,” *IEEE Trans. Signal Process.*, 2016 (submitted).
- [12] E. J. Candès, X. Li, and M. Soltanolkotabi, “Phase retrieval from coded diffraction patterns,” *Appl. Comput. Harmon. Anal.*, vol. 39, no. 2, pp. 277–299, Sep. 2015.
- [13] Y. Chen and E. J. Candès, “Solving random quadratic systems of equations is nearly as easy as solving linear systems,” in *Adv. Neural Inf. Process. Syst.*, Montreal, Canada, 2015, pp. 739–747.
- [14] G. Wang, G. B. Giannakis, and Y. C. Eldar, “Solving systems of random quadratic equations via truncated amplitude flow,” *arXiv:1605.08285*, 2016.
- [15] R. Balan, P. Casazza, and D. Edidin, “On signal reconstruction without phase,” *Appl. Comput. Harmon. Anal.*, vol. 20, no. 3, pp. 345–356, May 2006.
- [16] A. Conca, D. Edidin, M. Hering, and C. Vinzant, “An algebraic characterization of injectivity in phase retrieval,” *Appl. Comput. Harmon. Anal.*, vol. 38, no. 2, pp. 346–356, Mar. 2015.
- [17] A. Ben-Tal and A. Nemirovski, *Lectures on Modern Convex Optimization: Analysis, Algorithms, and Engineering Applications*. SIAM, 2001, vol. 2.
- [18] Y. Chen, X. Yi, and C. Caramanis, “A convex formulation for mixed regression with two components: Minimax optimal rates,” in *Proc. of The 27th Conf. on Learn. Theory*, Paris, France, June 2014, pp. 560–604.
- [19] H. Sahinoglou and S. D. Cabrera, “On phase retrieval of finite-length sequences using the initial time sample,” *IEEE Trans. Circuits and Syst.*, vol. 38, no. 8, pp. 954–958, Aug. 1991.
- [20] E. J. Candès, T. Strohmer, and V. Voroninski, “PhaseLift: Exact and stable signal recovery from magnitude measurements via convex programming,” *Appl. Comput. Harmon. Anal.*, vol. 66, no. 8, pp. 1241–1274, 2013.
- [21] J. Sun, Q. Qu, and J. Wright, “A geometric analysis of phase retrieval,” *arXiv:1602.06664*, 2016.
- [22] R. Kolte and S. A. Ozgur, “Phase retrieval via incremental truncated Wirtinger flow,” *arXiv:1606.03196*, 2016.
- [23] K. G. Murty and S. N. Kabadi, “Some NP-complete problems in quadratic and nonlinear programming,” *Math. Prog.*, vol. 39, no. 2, pp. 117–129, 1987.

- [24] R. Ge, F. Huang, C. Jin, and Y. Yuan, “Escaping from saddle points—Online stochastic gradient for tensor decomposition,” in *Proc. of The 28th Conf. on Learn. Theory*, 2015, pp. 797–842.
- [25] R. W. Gerchberg and W. O. Saxton, “A practical algorithm for the determination of phase from image and diffraction,” *Optik*, vol. 35, pp. 237–246, Nov. 1972.
- [26] G. Wang and G. B. Giannakis, “Solving random systems of quadratic equations via truncated generalized gradient flow,” in *Adv. Neural Inf. Process. Syst.*, Barcelona, Spain, 2016 (to appear).
- [27] B. Gao and Z. Xu, “Phase retrieval using Gauss-Newton method,” *arXiv:1606.08135*, 2016.
- [28] K. Wei, “Solving systems of phaseless equations via Kaczmarz methods: A proof of concept study,” *Inverse Probl.*, vol. 31, no. 12, p. 125008, Nov. 2015.
- [29] I. Waldspurger, A. d’Aspremont, and S. Mallat, “Phase recovery, maxcut and complex semidefinite programming,” *Math. Prog.*, vol. 149, no. 1–2, pp. 47–81, 2015.
- [30] K. Huang, Y. C. Eldar, and N. D. Sidiropoulos, “Phase retrieval from 1D Fourier measurements: Convexity, uniqueness, and algorithms,” *arXiv:1603.05215*, 2016.
- [31] T. Cai, J. Fan, and T. Jiang, “Distributions of angles in random packing on spheres,” *J. Mach. Learn. Res.*, vol. 14, no. 1, pp. 1837–1864, Jan. 2013.
- [32] G. H. Golub and C. F. Van Loan, *Matrix Computations*. Johns Hopkins University Press, 2012, vol. 3.
- [33] O. Shamir, “Fast stochastic algorithms for SVD and PCA: Convergence properties and convexity,” in *The 33th Proc. of Intl. Conf. on Machine Learning*, New York City, NY, 2016.
- [34] E. Oja, “Simplified neuron model as a principal component analyzer,” *J. Math. Biol.*, vol. 15, no. 3, pp. 267–273, Nov. 1982.
- [35] R. Johnson and T. Zhang, “Accelerating stochastic gradient descent using predictive variance reduction,” in *Adv. Neural Inf. Process. Syst.*, 2013, pp. 315–323.
- [36] S. Kaczmarz, “Angenherte auflösung von systemen linearer gleichungen,” *Bulletin International de l’Académie Polonaise des Sciences et des Lettres. Classe des Sciences Mathématiques et Naturelles. Série A, Sciences Mathématiques*, vol. 37, pp. 355–357, 1937.
- [37] P. M. Pardalos and S. A. Vavasis, “Quadratic programming with one negative eigenvalue is NP-hard,” *J. Global Optim.*, vol. 1, no. 1, pp. 15–22, 1991.
- [38] F. H. Clarke, “Generalized gradients and applications,” *T. Am. Math. Soc.*, vol. 205, pp. 247–262, 1975.
- [39] D. K. Berberidis, V. Kekatos, G. Wang, and G. B. Giannakis, “Adaptive censoring for large-scale regressions,” in *IEEE Intl. Conf. Acoustics, Speech and Signal Process.*, South Brisbane, QLD, Australia, 2015, pp. 5475–5479.



- [40] G. Wang, D. Berberidis, V. Kekatos, and G. B. Giannakis, "Online reconstruction from big data via compressive censoring," in *IEEE Global Conf. Signal and Inf. Process.*, Atlanta, GA, 2014, pp. 326–330.
- [41] R. Vershynin, "Introduction to the non-asymptotic analysis of random matrices," *arXiv:1011.3027*, 2010.
- [42] T. Strohmer and R. Vershynin, "A randomized Kaczmarz algorithm with exponential convergence," *J. Fourier Anal. Appl.*, vol. 15, no. 2, pp. 262–278, 2009.